

# Langevin-driven Pseudorandom Number Generator-induced Synchronization and Chaos

Jacob Jeffries  
Clemson University  
Department of Physics and Astronomy

# Contents

<b>1</b>	<b>Introduction</b>	<b>1</b>
1.1	Synchronization and Pseudorandom Number Generators . . . . .	1
1.2	The Maximal Lyapunov Exponent . . . . .	2
<b>2</b>	<b>Methods</b>	<b>4</b>
2.1	Calculating the MLE . . . . .	4
2.2	Quantifying Synchronization . . . . .	8
<b>3</b>	<b>Results</b>	<b>10</b>
3.1	Synchronization Time and Lyapunov Time for Two Highly Symmetric Potentials . . . . .	10
3.2	Anomalous Behavior of Asymmetric Potentials . . . . .	12
<b>4</b>	<b>Conclusions and Future Work</b>	<b>16</b>
4.1	Conclusions . . . . .	16
4.2	Future Work . . . . .	16

# List of Figures

2.1	Example PES. The system parameters used appear in Table 2.1. . . . .	5
2.2	Repeated sampling of $\eta$ to calculate $\lambda_{t^*}(\varphi_{\text{init}})$ . The equations of motion were integrated with a Verlet-type integration scheme [1]. Data are presented as 2D histogram to show long-term divergence from the average trajectory. The system parameters used appear in Table 3.2. . . . .	7
2.3	Synchronization time calculated from variations in each coordinate over 50 trajectories. The system parameters used appear in Table 3.2 with $\gamma = 10^{-1.7}$ . The top row represents variations in position with time, and the bottom row represents variations in momentum with time, where each column is a coordinate in configuration space. . . . .	9
3.1	LSP for the weak (left) and strong (right) tetrahedral potentials. . . . .	11
3.2	LSP for the weak (left) and strong (right) octahedral potentials. . . . .	11
3.3	LSP for a system with an asymmetric showing a correlation similar to symmetric potentials. The potential parameters used are shown in Table 3.3. . . . .	12
3.4	LSP for an anomalous system showing spiking behavior. Used potential parameters appear in Table 3.4. . . . .	13
3.5	LSPs for anomalous systems showing a negative relationship between $t_{\text{sync}}$ and $t_{\text{Ly}\alpha}$ . . . . .	14
3.6	LSPs showing spiking behavior. . . . .	15
3.7	LSPs showing complex patterns. . . . .	15

# List of Tables

2.1	PES parameters for an example PES.	5
2.2	System parameters for example Lyapunov exponent calculation.	7
3.1	PES parameters for the weak (left) and strong (right) tetrahedral potentials.	10
3.2	PES parameters for the weak (left) and strong (right) octahedral potentials.	10
3.3	PES parameters for a randomly generated asymmetric potential.	13
3.4	PES parameters for another randomly generated asymmetric potential.	14

## **Abstract**

Molecular dynamics (MD) simulations exhibit synchronization when using stochastic thermostats, of which are traditionally implemented with pseudorandom number generators (PRNGs). We used Lyapunov times to characterize synchronization on a toy potential constructed with Gaussian wells, and constructed both symmetric and randomly generated, asymmetric potentials. We found that, for our tested symmetric potentials, one can avoid synchronization by picking a friction coefficient lower than a critical friction coefficient, characterized by correlations between the Lyapunov time and synchronization time. This relationship breaks down, becoming much more complicated for the tested asymmetric potentials.

# Section 1

## Introduction

### 1.1 Synchronization and Pseudorandom Number Generators

MD simulations are often driven by stochastic thermostats to model a canonical ensemble [2]. This is traditionally implemented by choosing Gaussian-distributed numbers from a sequence generated by a pseudorandom number generator (PRNG).

Inadequacies in PRNGs lead to correlations between two initially independent trajectories. One artificial correlation is *synchronization*, which is the tendency for two initially independent trajectories  $\varphi_1$  and  $\varphi_2$  to become asymptotically equal in phase space:

$$\lim_{t \rightarrow \infty} \|\varphi_1(t) - \varphi_2(t)\| = 0 \quad (1.1)$$

where  $t$  is time and  $\|\cdot\|$  is the Euclidean norm. Synchronization rates for identical-noise trajectories have been analytically found for a harmonic well [3]. There also exists numerical evidence for synchronization in more complex systems [4].

Commonly used PRNGs often generate sequences with numbers only depending on the previous number in the sequence, or equivalently:

$$a_{n+1} = f(a_n) \quad (1.2)$$

This form of a PRNG guarantees periodicity since, given some seed  $a_k$  for a function  $f$  with discrete support:

$$a_{k+N} = \underbrace{(f \circ \cdots \circ f)}_{N \text{ times}}(a_k) \quad (1.3)$$

Considering two different sequences  $b_n$  and  $c_n$  (each with a finite number of discrete states) with seeds  $b_0$  and  $c_0$ . If there exists any two non-negative integers  $\ell$  and  $m$  such that  $b_\ell = c_m$  then  $b_{\ell+N} = c_{m+N}$  for any non-negative value of  $N$ . This results in two sequences that are aligned with lag. In the case that  $\ell = m$ , these two sequences are perfectly aligned.

One such PRNG is the linear congruential generator (LCG) [5]:

$$x_{n+1} = (ax_n + c) \mod m \quad (1.4)$$

where  $a$  is often called the multiplier,  $c$  the increment,  $m$  the modulus, and  $x_0$  the seed [6]. Note that the LCG generates a sequence of integers  $s$  such that  $\inf s = 0$  and  $\sup s = m - 1$ . One can then create a sequence of numbers approximately uniformly distributed over  $(0, 1)$  via the following transformation:

$$s_i'' = \frac{s_i + 1}{m + 1} \quad (1.5)$$

Note that  $\inf s'' = 1/(m + 1)$  and  $\sup s'' = m/(m + 1)$ , so for large  $m$  the sequence is bounded between 0 and 1.

With two distributions  $s_1''$  and  $s_2''$  that are independently and identically distributed uniformly over  $(0, 1)$ , one can then calculate a new sequence of numbers  $g$  that is uniformly distributed with zero mean and unit variance with the Box-Muller transform [7]:

$$g = \sqrt{-2 \ln s_1''} \cos 2\pi s_2'' \quad (1.6)$$

This sequence can then be scaled and shifted appropriately to some desired mean  $\mu$  and variance  $v^2$ :

$$g' = |v|g + \mu \quad (1.7)$$

## 1.2 The Maximal Lyapunov Exponent

Consider the following system over phase space  $\Omega \subseteq \mathbb{R}^n$ :

$$\dot{\varphi} = f(\varphi, t) \text{ such that } \varphi(0) = \varphi_{\text{init}} \quad (1.8)$$

where  $\varphi$  is a state vector in  $n$ -dimensional phase space,  $f$  is a component-wise-smooth vector field, and  $t$  is time. Now consider an initial small perturbation  $z(0)$  such that  $\varphi'(0) = \varphi(0) + z(0)$ . This defines two time series, the unperturbed time series  $\varphi(t)$  and the perturbed time series  $\varphi(t)$ , whose difference trajectory is  $z(t) = \varphi(t) - \varphi(0)$ .

For chaotic trajectories, this difference trajectory grows in time in magnitude. Conversely, for trajectories that converge, the difference trajectory shrinks in time in magnitude. The *maximal Lyapunov exponent* (LE) [8], which measures the exponential growth rate that dominates the difference trajectory  $z$  over long timescales caused by an infinitesimal initial perturbation, is defined as:

$$\begin{aligned} \lambda &= \lim_{t \rightarrow \infty} \lim_{\|z(0)\| \rightarrow 0^+} \frac{1}{t} \ln \frac{\|z(t)\|}{\|z(0)\|} \\ &= \lim_{t' \rightarrow \infty} \lim_{\|z(0)\| \rightarrow 0^+} \frac{1}{t'} \int_0^{t'} \frac{d}{dt} \ln \frac{\|z(t)\|}{\|z(0)\|} dt \\ &= \lim_{\|z(0)\| \rightarrow 0^+} \left\langle \frac{d}{dt} \ln \frac{\|z(t)\|}{\|z(0)\|} \right\rangle_{t \in \mathbb{R}^+} \end{aligned} \quad (1.9)$$

Assuming ergodicity, this is equivalent to an average over phase space  $\Gamma$ :

$$\lambda = \lim_{\|z(0)\| \rightarrow 0^+} \left\langle \frac{d}{dt} \ln \frac{\|z(t)\|}{\|z(0)\|} \right\rangle_{\Gamma} \quad (1.10)$$

This formulation is advantageous because (1.9) is problematic in practice. The MLE is a dynamical invariant [9], with the possibility for numerical overflow for chaotic systems (where the MLE is positive) on long time-scales, since:

$$\|z(t)\| \sim \|z(0)\|e^{\lambda t} \quad (1.11)$$

which quickly tends to infinity for any finite  $\|z(0)\|$  and  $\lambda > 0$ . (1.10) is a remedy for this since one can average over local quantities calculated over small time intervals, provided that one can be confident that the necessary finite- $\|z(0)\|$  approximation holds over those small time intervals. Notably, reformulating the MLE in terms of phase space averages also turns the MLE calculation into an embarrassingly parallel problem.

# Section 2

## Methods

### 2.1 Calculating the MLE

The Langevin equation describes systems driven by a Langevin thermostat:

$$m\ddot{q} = -\nabla V(q) - \gamma m\dot{q} + \sqrt{2m\gamma\beta^{-1}} R(t) \quad (2.1)$$

where  $q$  is position in  $\mathbb{R}^d$ ,  $\nabla$  is the gradient in configuration space,  $V$  is the potential-energy-surface (PES),  $\gamma$  is a dampening constant,  $\beta^{-1} = k_B T$  is the thermal energy provided by the thermostat,  $t$  is time, and  $R(t)$  is a stationary, delta-correlated Gaussian process which models coupling with a large temperature reservoir. Here, we set  $m = \beta = 1$ , so:

$$\ddot{q} = -\nabla V(q) - \gamma\dot{q} + \sqrt{2\gamma} R(t) \quad (2.2)$$

Or, equivalently as a first order system:

$$\begin{aligned} \dot{q} &= p \\ \dot{p} &= -\nabla V(q) - \gamma p + \sqrt{2\gamma} R(t) \end{aligned} \quad (2.3)$$

To study this system, we construct a PES from Gaussian wells:

$$V_{\text{gauss}}(q) = \sum_i h_i \exp\left(\frac{-\|q - m_i\|^2}{2\sigma_i^2}\right) \quad (2.4)$$

The system is then confined in a harmonic super-basin:

$$V_{\text{basin}}(q) = \frac{1}{2} \left( \sum_i \sigma_i \right)^{-2} \|q - \langle m \rangle\|^2 \quad (2.5)$$

where  $\langle m \rangle$  is the component-wise mean of  $\{m_i\}$ . The total potential is thus:

$$V(q) = V_{\text{gauss}}(q) + V_{\text{basin}}(q) \quad (2.6)$$

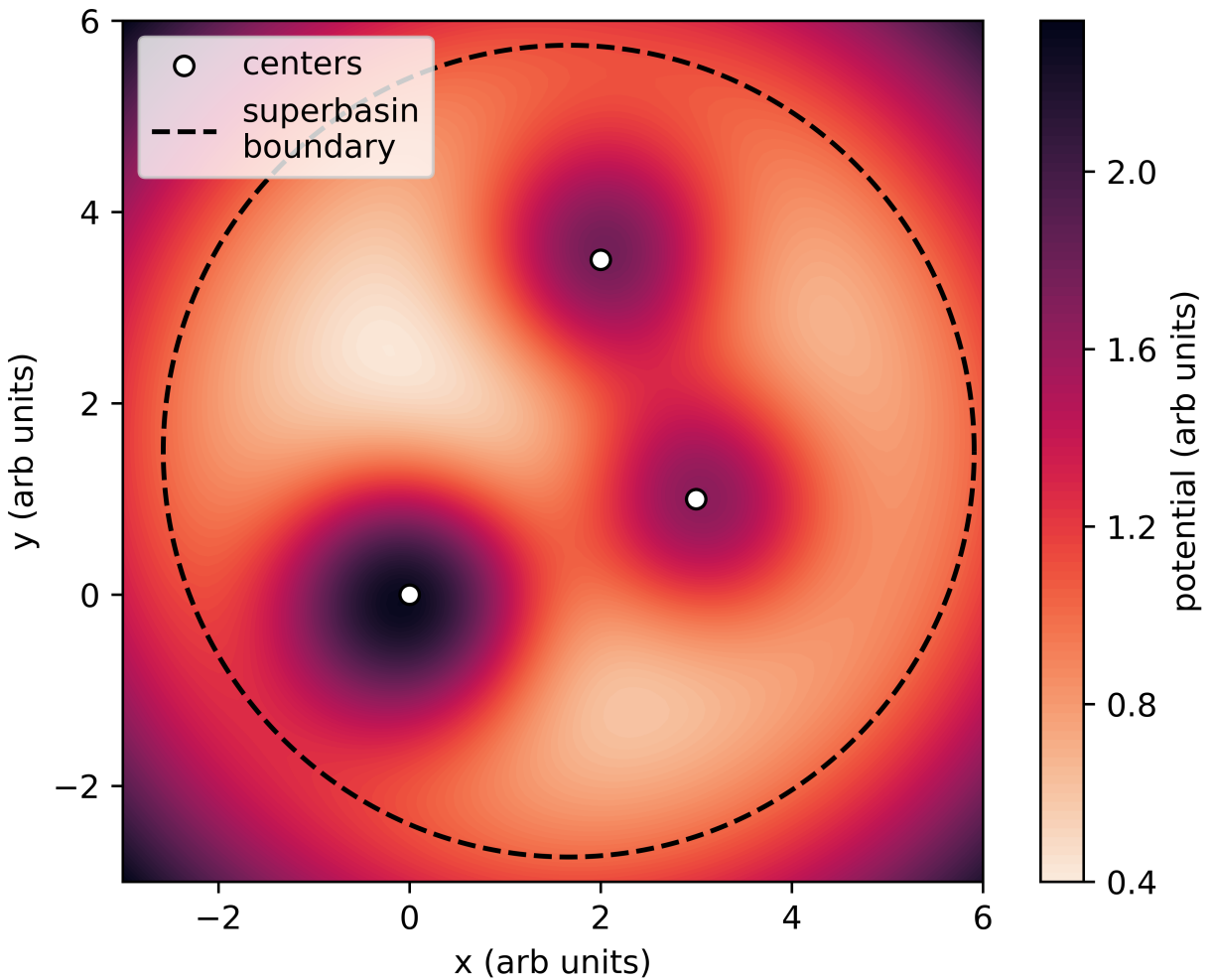


Figure 2.1: Example PES. The system parameters used appear in Table 2.1.

heights	[2.0, 1.5, 1.5]
centers	[0.0, 0.0] [3.0, 1.0] [2.0, 3.5]
widths	[1.0, 1.0, 1.0]

Table 2.1: PES parameters for an example PES.

We also define the phase space vector  $\varphi$  as  $(q \quad \xi p)^\top$  where  $p$  is momentum and  $\xi$  is an arbitrary scaling factor such that  $\|\varphi\|$  is well-defined. For the remainder of this work, we set  $\xi = 1$ .

One can calculate two trajectories  $\varphi(t)$  and  $\varphi'(t)$  simultaneously by perturbing the initial condition by some small-normed vector  $z(0) = \eta$ :

$$\begin{aligned}\dot{\varphi} &= f(\varphi, t) \text{ such that } \varphi(0) = (q_0 \quad \xi p_0)^\top \\ \varphi' &= f(\varphi', t) \text{ such that } \varphi'(0) = \varphi(0) + \eta\end{aligned}\tag{2.7}$$

where  $f$  is implicitly defined by (2.2).

If  $\|\eta\|$  is nonzero,  $\ln \delta(t) = \ln \|\varphi(t) - \varphi'(t)\|$  will be approximately linear for some finite value of time  $t^*$ . The slope  $\lambda_{t^*}(\varphi(0))$  of this linear region can be calculated by (Figure 2.2):

- Choose multiple perturbation vectors  $\{\eta_1, \eta_2, \dots\}$  with fixed magnitude  $\|\eta_k\| = \varepsilon$  for all  $k$
- For each  $\eta_i \in \{\eta_1, \eta_2, \dots\}$  at some fixed initial point  $\varphi(0) = \varphi_{\text{init}}$ 
  - Time-evolve (2.7) with  $\eta = \eta_i$  to obtain both  $\varphi(t)$  and  $\varphi'(t)$
  - Calculate  $\ln \delta_i(t) = \ln \|\varphi(t) - \varphi'(t)\|$
- Calculate the expected time series  $E(t) = \langle \ln \delta_i(t) \rangle_i$
- Find  $t^*$  such that, for some tolerance  $M$  (note that the condition is equivalent to a linear regression):

$$t^* = \sup \left\{ \zeta : \min_{a,b} \|y_{ab} - E\|_{[0,\zeta]} < M \right\} \tag{2.8}$$

- Calculating the finite-time MLE  $\lambda_{t^*}(\varphi(0))$ :

$$(a_{\text{opt}} \quad \lambda_{t^*}(\varphi_{\text{init}}))^\top = \arg \min_{a,b} \|y_{ab} - E\|_{[0,t^*]} \tag{2.9}$$

where  $y_{ab}(t) = a + bt$  and  $\|\cdot\|_{\mathcal{T}}$  is some function norm over the interval  $\mathcal{T}$ , e.g. the  $L^2$  norm implemented here:

$$\|g\|_{\mathcal{T}} = \sqrt{\int_{\mathcal{T}} |g(t)|^2 dt} \tag{2.10}$$

The conditions in (2.8) and (2.9) were achieved by performing a linear regression starting at  $t = 0$  and consecutively ending at a later time  $t = T$  (incrementing by a timestep) until  $r^2$  for the linear regression was less than 95%.

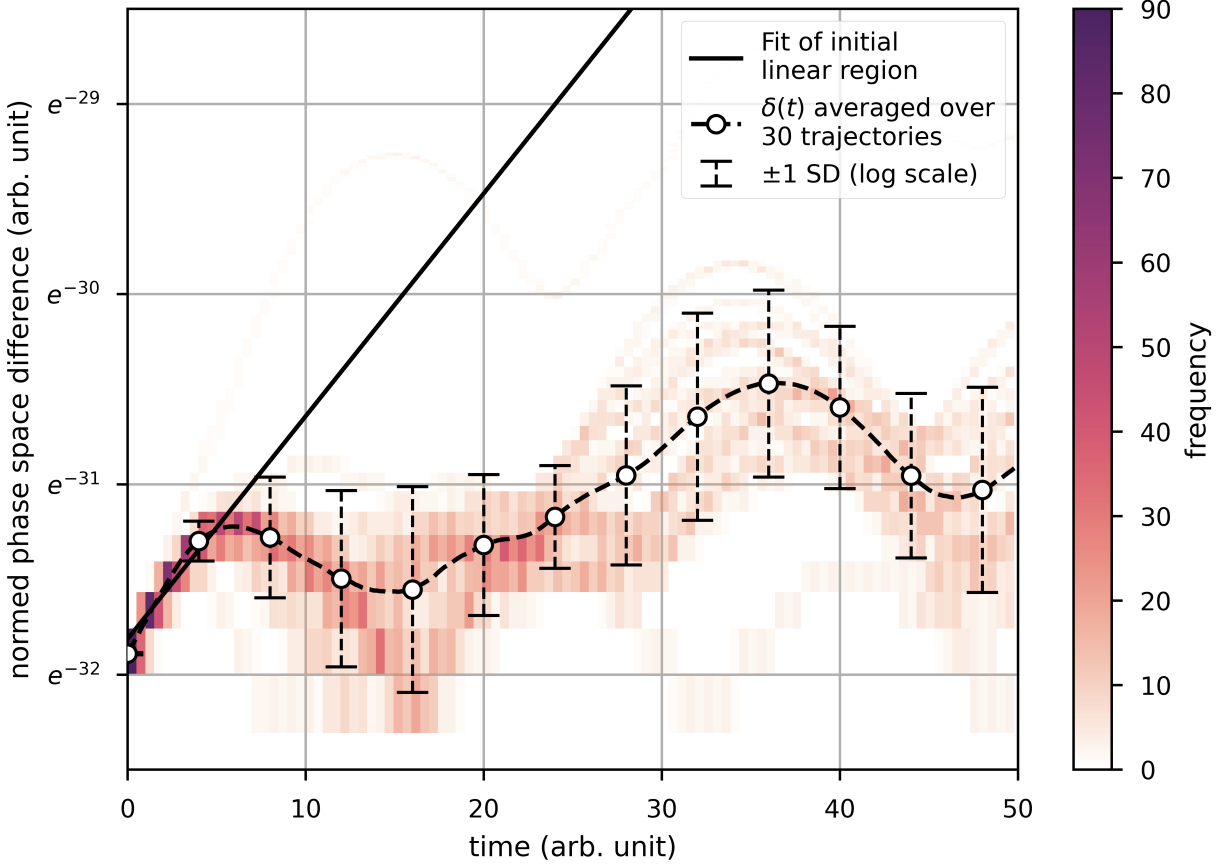


Figure 2.2: Repeated sampling of  $\eta$  to calculate  $\lambda_{t^*}(\varphi_{\text{init}})$ . The equations of motion were integrated with a Verlet-type integration scheme [1]. Data are presented as 2D histogram to show long-term divergence from the average trajectory. The system parameters used appear in Table 3.2.

$\{h_i\}$	[1.0, 0.5, 1.2]
$\{m_i\}$	[1.0, 0.0, 3.0]
$\{\sigma_i\}$	[0.0, 0.0, 0.0]
$\{\sigma_i\}$	[0.0, 2.0, 0.0]
$\varphi_{\text{init}}$	[1.0, 1.0, 1.0]
$\gamma$	[0.0, 0.0, 0.1, 0.0, 0.0, 0.0]
	0

Table 2.2: System parameters for example Lyapunov exponent calculation.

Repeating this process by sampling over all of phase space, (1.10) then allows for the calculation of the global, system-wide LE:

$$\lambda = \lim_{\varepsilon \rightarrow 0^+} \left\langle \lambda_{t^*}(\varphi_{\text{init}}) \right\rangle_{\varphi_{\text{init}} \in \Gamma} \quad (2.11)$$

where states are expected to be Boltzmann-distributed since the Langevin equation imposes a long-term,

absolute temperature, so states can be efficiently sampled from a Boltzmann distribution. This was achieved by uniform sampling in configuration space (inside the super-basin) and Gaussian sampling in momentum space, then weighting each measurement with a Boltzmann weight with respect to configuration space:

$$\lambda = \lim_{\varepsilon \rightarrow 0^+} \frac{\int_C e^{-V(q)} \lambda_{t^*}(q, p) \Big|_{p \text{ from } \mathcal{N}(0, 2mI_d)} d^d q}{\int_C e^{-V(q)} d^d q} \quad (2.12)$$

where  $I_d$  is the  $d$ -by- $d$  identity matrix and  $\mathcal{N}(\mu, \Sigma)$  is the multivariate normal distribution with mean  $\mu$  and covariance matrix  $\Sigma$ .

The *Lyapunov time*  $t_{\text{Ly}}$  is then defined as  $\lambda^{-1}$ , (for  $\lambda > 0$ ) which measures the timescale at which the system becomes measurably chaotic, or more precisely the characteristic  $e$ -folding time.

## 2.2 Quantifying Synchronization

Suppose there exist  $N$  trajectories  $(\varphi_1, \dots, \varphi_n)$  subject to the same potential and thermostat. At  $t = 0$ , each trajectory has a distinct state (randomly sampled over at-rest configuration space in our case).

At each time  $t > 0$ , each trajectory has a state defined by its time-evolved coordinates. For synchronization to occur over some time interval  $\mathcal{T}$ , each trajectory needs to share an identical set of coordinates for all  $t \in \mathcal{T}$ .

By nature of numerical integration, once the trajectories become synchronized within floating-point accuracy, they cannot become desynchronized, so the time interval of interest is of the form  $\mathcal{T} = (t_{\text{sync}}, \infty) \subset \mathbb{R}^+$  for some  $t_{\text{sync}} \in \mathbb{R}^+$ . Equivalently, the synchronization time  $t_{\text{sync}}$  is defined as  $\inf \mathcal{T}$ , where  $\mathcal{T}$  is the time interval such that all  $N$  trajectories are permanently synchronized.

This can be measured to be the interval such that the standard deviation of all coordinates between trajectories is below some threshold  $\varepsilon$ :

$$t_{\text{sync}} = \inf \left\{ t : \frac{1}{N} \sum_i \|\varphi_i(t) - \langle \varphi(t) \rangle\|^2 < \varepsilon^2 \right\} \quad (2.13)$$

If the above set is the empty set (i.e. if the trajectories never synchronize), then  $t_{\text{sync}}$  is defined to be  $\infty$ .

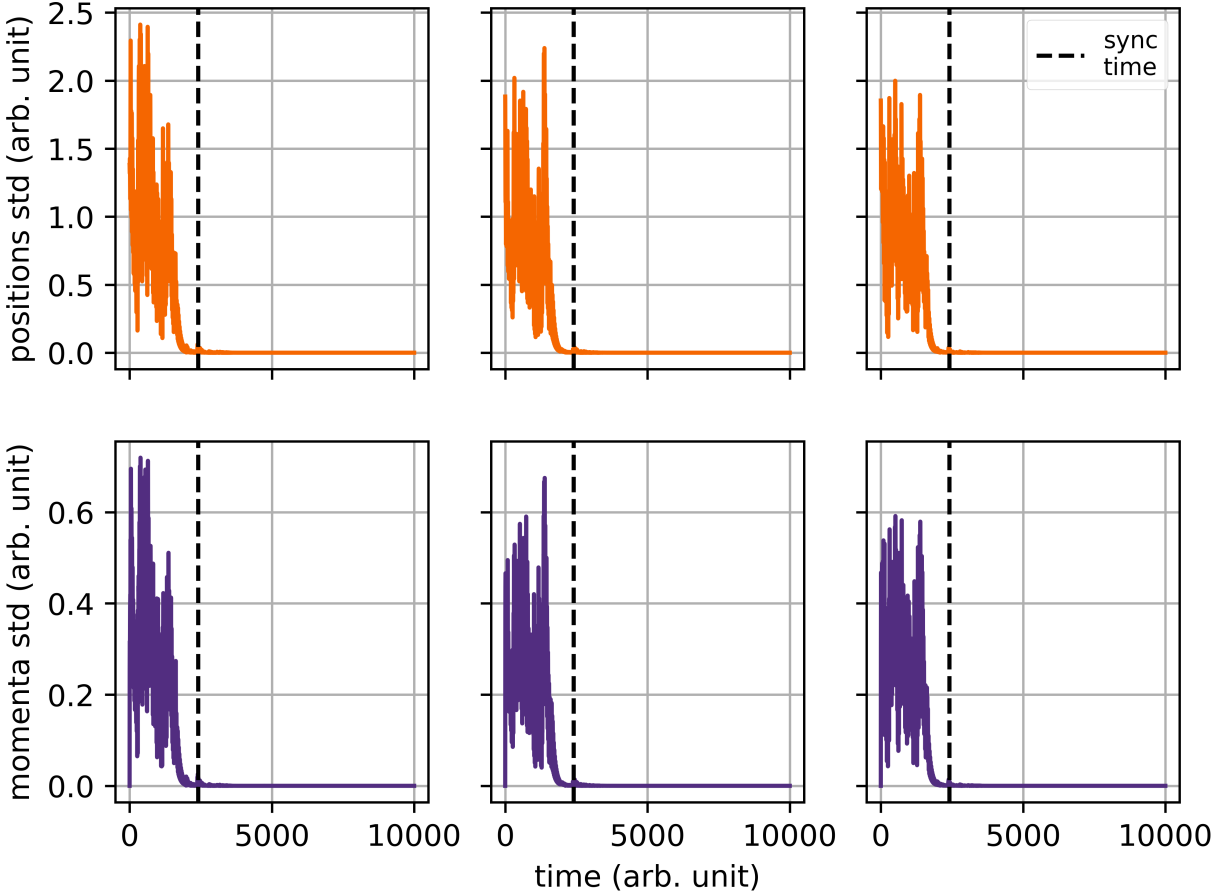


Figure 2.3: Synchronization time calculated from variations in each coordinate over 50 trajectories. The system parameters used appear in Table 3.2 with  $\gamma = 10^{-1.7}$ . The top row represents variations in position with time, and the bottom row represents variations in momentum with time, where each column is a coordinate in configuration space.

The threshold  $\varepsilon^2$  should be different for each type of state coordinate. In our case, this was taken to be 5% of  $\langle \sigma \rangle$  for position and 5% of  $\sqrt{m\beta^{-1}} = \sqrt{m}$  for momentum (Figure 2.3):

$$t_{\text{sync}} = \inf \left\{ t : \frac{1}{N} \sum_i \|q_i(t) - \langle q(t) \rangle\|^2 < (0.05\langle \sigma \rangle)^2 \text{ and } \frac{1}{N} \sum_i \|p_i(t) - \langle p(t) \rangle\|^2 < (0.05\sqrt{m})^2 \right\} \quad (2.14)$$

For trajectories that do not synchronize (which occurs at large friction coefficients), the synchronization time is defined to be infinite. In the results, this is presented as  $t_{\text{sync}} = t_{\text{sim}}$ , where  $t_{\text{sim}}$  is the total simulation time.

Furthermore, at large friction coefficients, synchronization can strongly effect short-term dynamics. In this limit, the previously discussed method for calculating  $t_{\text{Ly}\alpha}$  is no longer valid, given that  $\ln \delta(t)$  is undefined when  $\delta(t) = 0$ , which can occur on the short timescales considered in the methodology.

## Section 3

# Results

### 3.1 Synchronization Time and Lyapunov Time for Two Highly Symmetric Potentials

To test how the synchronization time and Lyapunov time correlate, we construct two highly symmetric potentials. These two potentials are denoted by polygons (specifically a tetrahedron and an octahedron), with barriers of height  $h$  at each vertex of the polygon. We also consider the cases where  $h$  is weak compared to the thermostat ( $h = \beta^{-1} = 1$ ), as well as strong compared to the thermostat ( $h = 5\beta^{-1} = 5$ ).

heights	[1.0, 1.0, 1.0, 1.0]	heights	[5.0, 5.0, 5.0, 5.0]
	[1.0, 0.0, -0.707]		[1.0, 0.0, -0.707]
centers	[-1.0, 0.0, -0.707]	centers	[-1.0, 0.0, -0.707]
	[0.0, 1.0, 0.707]		[0.0, 1.0, 0.707]
	[0.0, -1.0, 0.707]		[0.0, -1.0, 0.707]
widths	[0.5, 0.5, 0.5]	widths	[0.5, 0.5, 0.5, 0.5]

Table 3.1: PES parameters for the weak (left) and strong (right) tetrahedral potentials.

heights	[1.0, 1.0, 1.0, 1.0, 1.0, 1.0]	heights	[5.0, 5.0, 5.0, 5.0, 5.0, 5.0]
	[1.0, 0.0, 0]		[1.0, 0.0, 0]
centers	[-1.0, 0.0, 0]	centers	[-1.0, 0.0, 0]
	[0.0, 1.0, 0]		[0.0, 1.0, 0]
	[0.0, -1.0, 0]		[0.0, -1.0, 0]
	[0.0, 0.0, 1.0]		[0.0, 0.0, 1.0]
	[0.0, 0.0, -1.0]		[0.0, 0.0, -1.0]
widths	[0.5, 0.5, 0.5, 0.5, 0.5, 0.5]	widths	[0.5, 0.5, 0.5, 0.5, 0.5, 0.5]

Table 3.2: PES parameters for the weak (left) and strong (right) octahedral potentials.

To numerically experiment, the log-friction coefficient  $\log_{10} \gamma$  was varied from  $-2$  to  $-1$  with a step size of  $0.025$ . Our previously described scheme was then run for each value of  $\gamma$ , calculating a Lyapunov time and synchronization time for each value of  $\gamma$ . This generates a set of triplets  $\{(t_{\text{Ly}\alpha}, t_{\text{sync}}, \gamma)\}$ , and this entire set of triplets was generated for all four potential combinations. This set of triplets is dubbed to be the Lyapunov-synchronization profile (LSP) of that potential.

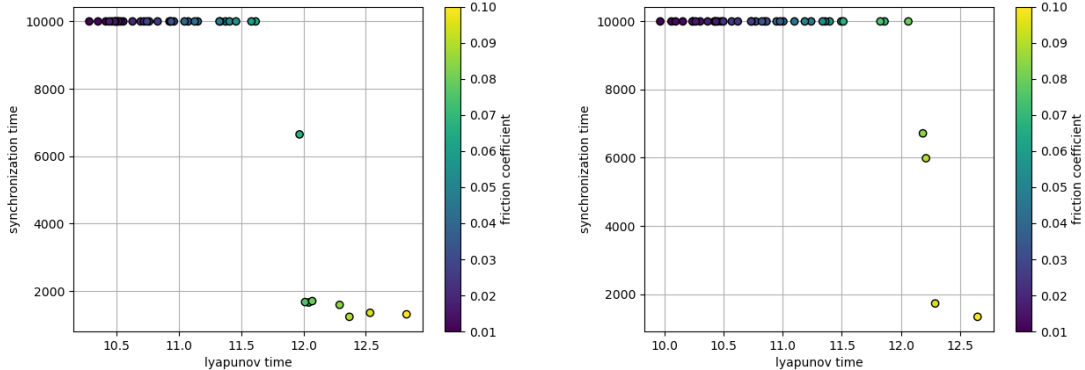


Figure 3.1: LSP for the weak (left) and strong (right) tetrahedral potentials.

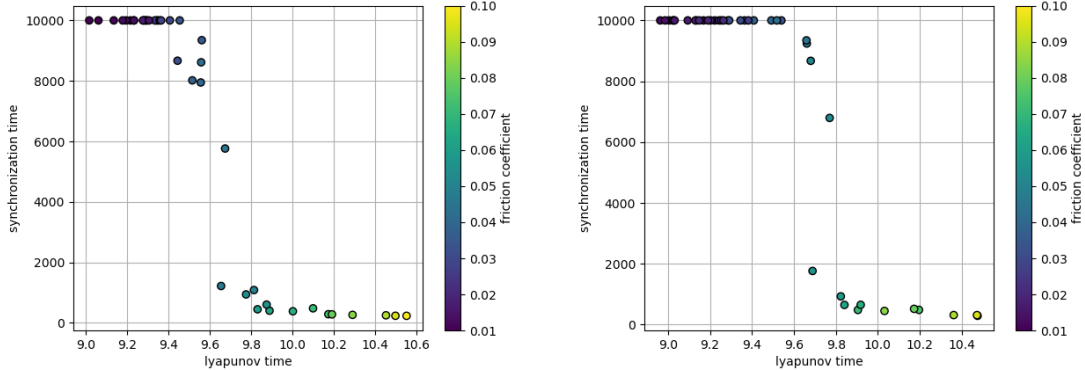


Figure 3.2: LSP for the weak (left) and strong (right) octahedral potentials.

For these highly symmetric systems, we see clear correlations between the two dynamical variables ( $t_{\text{Lya}}$  and  $t_{\text{sync}}$ ) as well as the input parameter  $\gamma$ . As one decreases the Lyapunov time (by decreasing the friction coefficient), the synchronization time approaches the simulation time (which was set to  $10^4$ ). Thus, synchronization never occurs for Lyapunov times below some critical Lyapunov time.

Intuitively,  $t_{\text{sync}}$  decreases with  $t_{\text{Lya}}$ , and decreases with  $\gamma$ . The relationship between  $t_{\text{sync}}$  and  $\gamma$  is certainly the more intuitive of the two:  $\gamma$  represents the strength of the thermostat, and increasing the strength of the thermostat should make two independent trajectories synchronize faster.

$t_{\text{Lya}}$  is a measurement of local divergence, in the sense that two infinitesimally close trajectories will diverge on the timescale  $t_{\text{Lya}}$ , while  $t_{\text{sync}}$  is a measurement of global convergence on long timescales. Here, we see a relationship between the two, i.e. global convergence on long timescales can be predicted by local divergence on short timescales for these highly symmetric potentials. We predict that this trend holds true for more realistic systems with highly symmetric potentials, such as crystal lattices.

Furthermore, we see that there exists some critical  $t_{\text{Lya}}^*$  that splits the LSP into two regions: the synchronizing region, where  $t_{\text{sync}} < t_{\text{sim}}$ , and the non-synchronizing region, where  $t_{\text{sync}} = t_{\text{sim}}$ .

Long term global convergence is problematic when creating statistically independent trajectories in molecular dynamical simulations, and thus limits the choice of friction coefficient  $\gamma$ . Due to the timescale problem of

molecular dynamics, probing long term global convergence for some  $\gamma$  is unrealistic on most hardware for some especially long processes, such as vacancy diffusion in solids.

If the results above extend to realistic systems, one can instead find  $t_{\text{Ly}}^*$  and its corresponding friction coefficient  $\gamma^*$ . One can then be confident that trajectories generated by friction coefficients significantly lower than  $\gamma^*$  will not synchronize. Thus, this work suggests a valuable method for avoiding synchronization at reduced computational expense.

### 3.2 Anomalous Behavior of Asymmetric Potentials

For asymmetric potentials, the aforementioned patterns no longer reliably hold. This was studied by generating random PESs, varying the number of Gaussian peaks (with unit width,  $\sigma_i = 1$ ) with random heights and positions.

For some systems, such as the 2-peak PES described in Table 3.3, the correlation still holds, but the shape of the LSP significantly changes (Fig 3.3). Here, the correlation between the synchronization time and the Lyapunov time remains, but the relationship between the Lyapunov time and the friction coefficient is no longer monotonic.

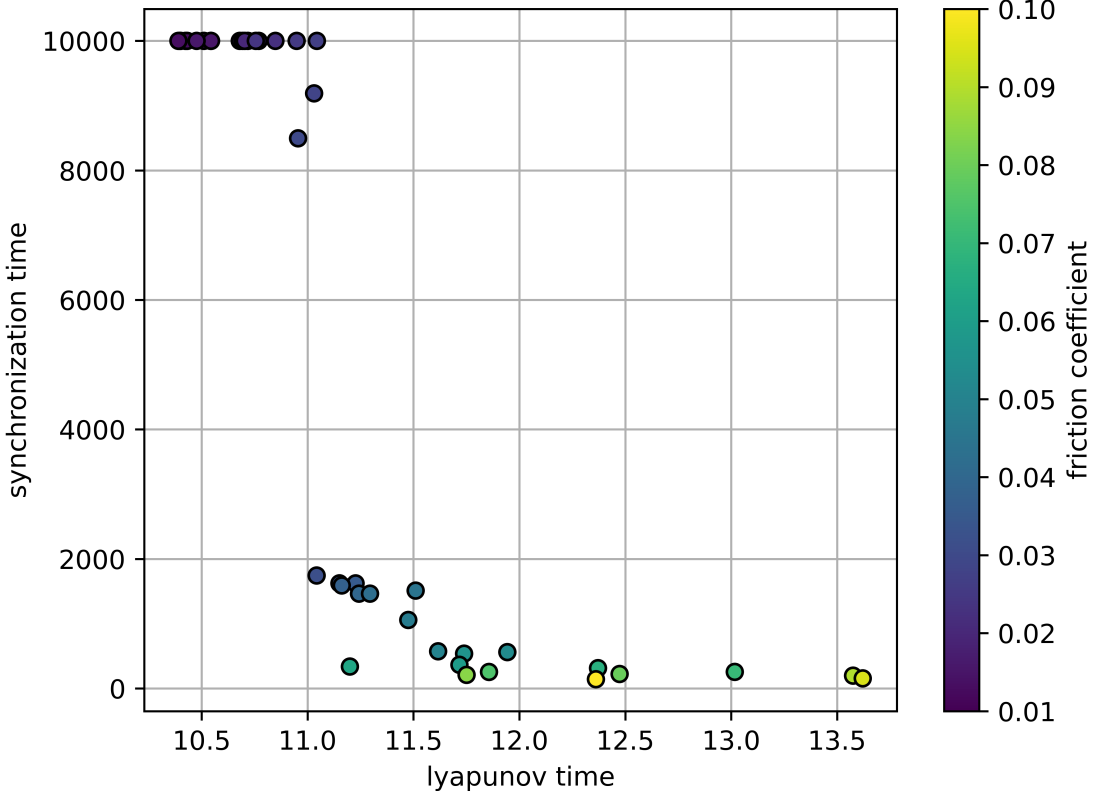


Figure 3.3: LSP for a system with an asymmetric showing a correlation similar to symmetric potentials. The potential parameters used are shown in Table 3.3.

heights	[2.0308590320374003, 0.07396304380289664]
centers	[0.7454106288280373, -2.280176336307992, -2.251840409241546] [2.9235067020707817, 0.7813778056446798, -1.7599240311742212]
widths	[1.0, 1.0]

Table 3.3: PES parameters for a randomly generated asymmetric potential.

Other systems show an odd, but clearly continuous pattern as  $\gamma$  changes (Figure 3.4). In these systems, as one decreases  $\gamma$ , the Lyapunov time starts at some high value, decreases, then increases towards some intermediate Lyapunov time, and then saturates. Note that there still exists a critical friction coefficient - but it is now much more difficult to identify from the Lyapunov time, so one cannot use a Lyapunov time calculation as a test for long-term synchronization.

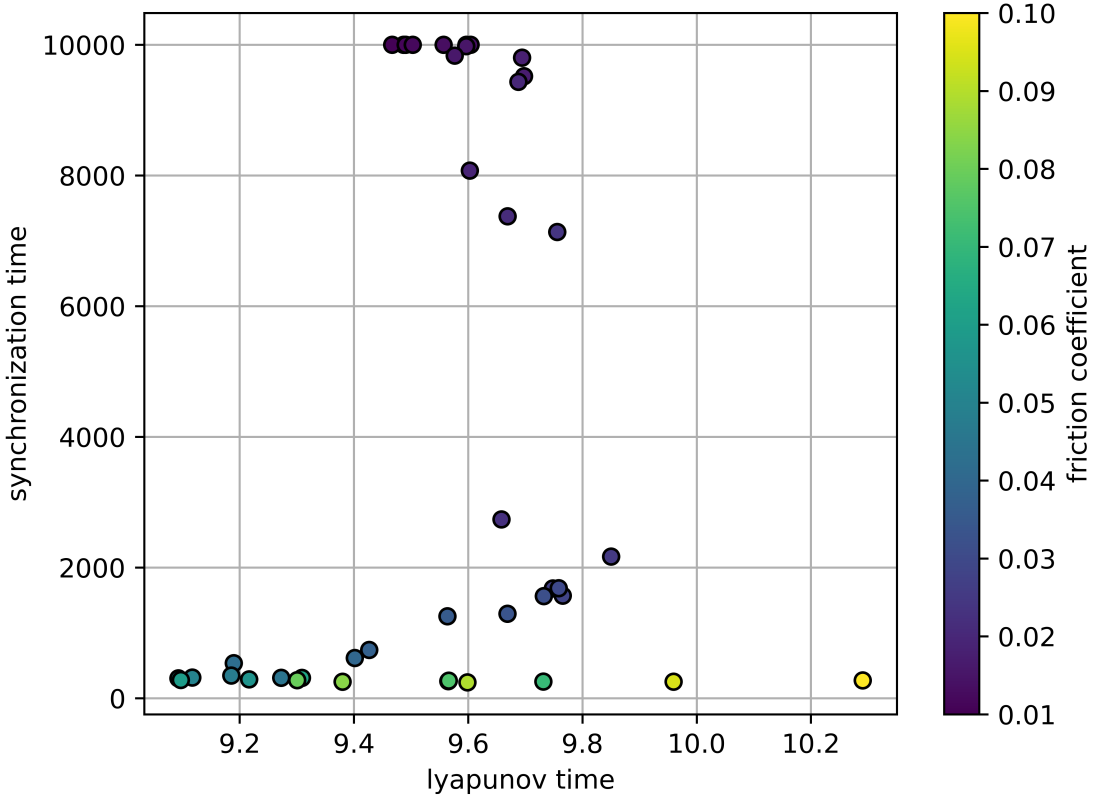


Figure 3.4: LSP for an anomalous system showing spiking behavior. Used potential parameters appear in Table 3.4.

heights	[1.5065865072000006, 2.719003400909431, 0.9594367401846882, 0.5981446780229457, 2.569805335145279, 2.087104432048627]
centers	[3.5101002185164774, -4.051693724059571, 0.18449214852474682] [2.855249282379237, -2.9893791216529952, 1.6706150195638898] [-0.8324656677213991, 1.027084695649613, 5.586684385597474] [-1.1193375861359165, -4.913074589765123, -1.347902259520108] [5.157154544416727, -5.155777045894599, 2.8935032531736287] [-4.111001830412666, 0.681594675624698, 2.516005902051127]
widths	[1.0, 1.0, 1.0, 1.0, 1.0, 1.0]

Table 3.4: PES parameters for another randomly generated asymmetric potential.

To experiment with asymmetric potentials, 70 different asymmetric PESs were randomly generated. Each potential has between 1 and 10 Gaussian wells with heights varying from 1 to 3 with unit widths. All the tested asymmetric systems seem to fall into one of three categories based on their LSPs:

- LSPs showing a nonlinear inverse relationship between  $t_{\text{sync}}$  and  $t_{\text{Ly}} \alpha$  with a non-monotonic relationship between  $\gamma$  and  $t_{\text{sync}}$  (Fig 3.5)
- LSPs showing “spiking” behavior ( $t_{\text{Ly}}$  saturating for at some constant for low  $t_{\text{sync}}$ ) (Fig 3.6)
- LSPs showing complex patterns (Fig 3.7)

Below are examples of LSPs for systems in each category.

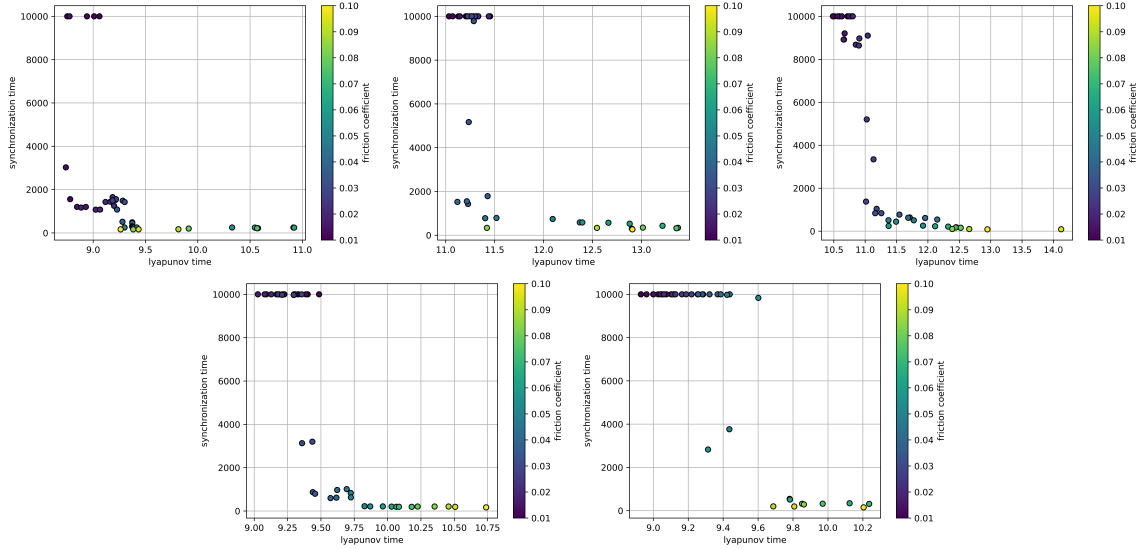


Figure 3.5: LSPs for anomalous systems showing a negative relationship between  $t_{\text{sync}}$  and  $t_{\text{Ly}}$ .

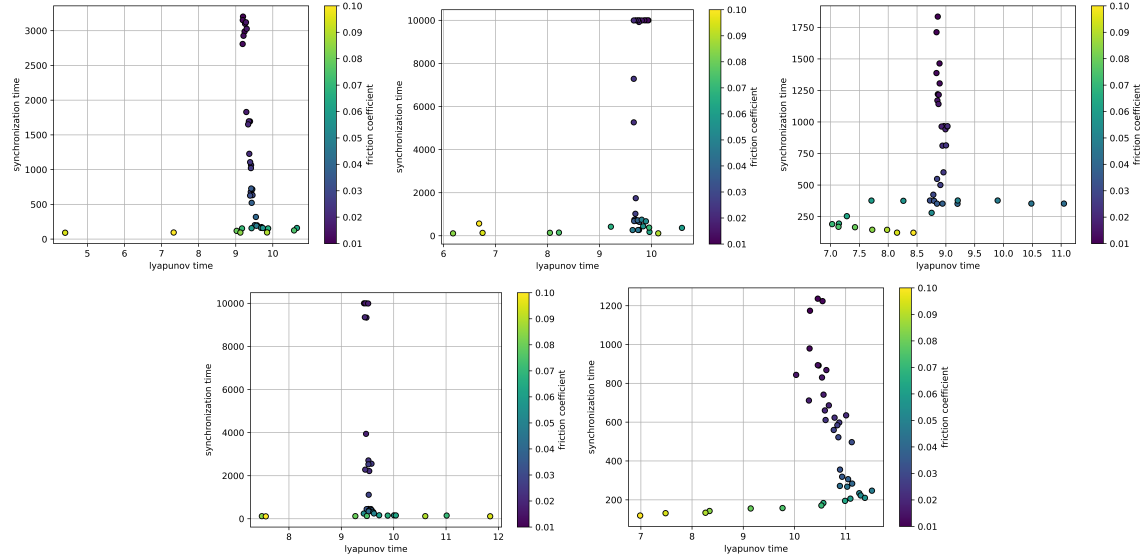


Figure 3.6: LSPs showing spiking behavior.

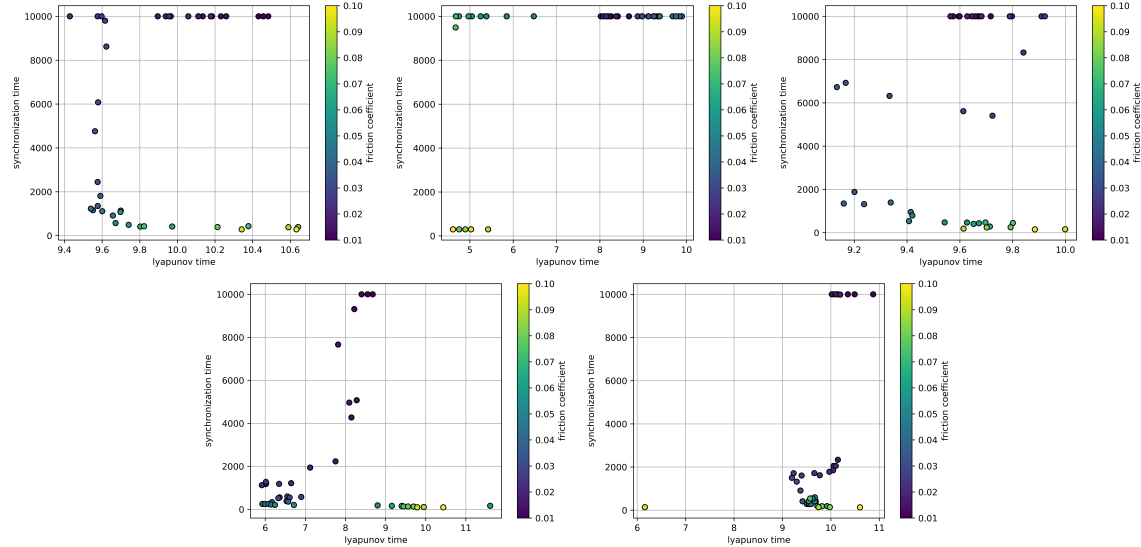


Figure 3.7: LSPs showing complex patterns.

All of the tested systems seem to still exhibit a critical friction coefficient. However, without a simple, predictable relationship between  $\gamma$ ,  $t_{\text{Lya}}$ , and  $t_{\text{sync}}$ , one cannot use  $t_{\text{Lya}}$  as a predictor of long-term synchronization.

## Section 4

# Conclusions and Future Work

### 4.1 Conclusions

We showed that, for our tested symmetric potentials, one can use the relationship between the synchronization time, and the Lyapunov time to identify a maximum friction coefficient that avoids long-term synchronization. Since the Lyapunov time can be calculated from averaged short-term dynamics (assuming ergodicity) from independent trajectories, one can probe (often inaccessible) long-term dynamics from a highly parallelizable calculation of the Lyapunov time. We expect that these results extend to more realistic systems, such as crystal lattices (which are symmetric by design).

This relationship between the synchronization time, the Lyapunov time and the friction coefficient breaks down for our tested asymmetric potentials. We similarly expect this to extend to more realistic systems, meaning one can only reliably use the aforementioned procedure (averaged short-term dynamics to probe long-term synchronization) for highly symmetric systems.

### 4.2 Future Work

In this work, our PRNG sequences were all initialized with the same seed. In practice, one would not use the same thermostat seed to obtain statistically independent trajectories.

However, two PRNGs could synchronize with lag given two different seeds. Consider two seeds,  $x_0$  and  $y_0$ . If members of each sequence  $(x_n)$  and  $(y_n)$  are equal with lag  $L$  at some step  $m$ :

$$x_m = y_{m+L} \tag{4.1}$$

Then:

$$y_{m+L+N} = (\underbrace{f \circ \cdots \circ f}_{N \text{ times}})(y_{m+L}) = (\underbrace{f \circ \cdots \circ f}_{N \text{ times}})(x_m) = x_{m+N} \tag{4.2}$$

so the two PRNG sequences are synchronized with lag  $L$ , introducing a correlation between two trajectories. Quantifying the relationship between synchronization and the Lyapunov time in this case is a much more complicated task, since:

- One needs to take into account the lag between the PRNG sequences, which is a nontrivial calculation

- One needs to take into account how the two seeds affect the relationship, since the lag will depend on the pair of seeds

However, we predict that a simulation with identical seeds is the “worst case scenario” for synchronization, i.e. one can use identical seeds to get an upper-bound on an appropriate friction coefficient for nonidentical seeds.

Additionally, for this method to be computationally viable, one must be able to calculate the critical friction coefficient without calculating the synchronization time. Here, the critical friction coefficient is characterized by a sharp change in the synchronization time, rather than some change in the Lyapunov time. Since there is a clear relationship between the two variables, we hypothesize that there exists a way to find this critical friction coefficient without calculating synchronization time.

Lastly, an obvious extension of this work is to perform a similar analysis on a more realistic system. A realistic system that maps well to our symmetric potentials is vacancy diffusion in a homogeneous crystal, where one tracks the vacancy as it moves through phase space, which is of interest when calculating quantities like the vacancy heat of transport [10].

# Bibliography

- [1] Benedict Leimkuhler and Charles Matthews. Robust and efficient configurational molecular sampling via langevin dynamics. *The Journal of Chemical Physics*, 138, 2013.
- [2] Philippe H. Hünenberger. *Thermostat Algorithms for Molecular Dynamics Simulations*, pages 105–149. Springer Berlin Heidelberg, Berlin, Heidelberg, 2005.
- [3] Blas P. Uberuaga, Marian Anghel, and Arthur F. Voter. Synchronization of trajectories in canonical molecular-dynamics simulations: Observation, explanation, and exploitation. *Journal of Chemical Physics*, 120, 2004.
- [4] Daniel J. Sindhikara, Seonah Kim, Arthur F. Voter, and Adrian E. Roitberg. Bad seeds sprout perilous dynamics: Stochastic thermostat induced trajectory synchronization in biomolecules. *Journal of Chemical Theory and Computation*, 5, 2008.
- [5] D. E. Knuth. *The Art of Computer Programming Volume 2: Seminumerical Algorithms*. Addison-Wesley, 1998.
- [6] A.M. Frieze, R. Kannan, and J.C. Lagarias. Linear congruential generators do not produce random sequences. *25th Annual Symposium on Foundations of Computer Science*, 1984.
- [7] William H. Press, Saul A. Teukolsky, William T. Vetterling, and Brian P. Flannery. *Numerical Recipes in C*. Cambridge University Press, Cambridge, USA, second edition, 1992.
- [8] Artur Dabrowski, Marek Balcerzak, Danylo Pikunov, and Andrzej Stefanski. Improving efficiency of the largest lyapunov exponent's estimation by its determination from the vector field properties. *Nonlinear Dynamics*, 102, 2020.
- [9] Joachim Holzfuss and Ulrich Parlitz. Lyapunov exponents from time series. In Ludwig Arnold, Hans Crauel, and Jean-Pierre Eckmann, editors, *Lyapunov Exponents*, pages 263–270, Berlin, Heidelberg, 1991. Springer Berlin Heidelberg.
- [10] Patrick K. Schelling, Jacques Ernouette, Lalit Shokeen, J. Woods Halley, and William C. Tucker. Molecular-dynamics calculation of the vacancy heat of transport. *Journal of Applied Physics*, 116, 2014.